PAW: Data Partitioning Meets Workload Variance

Zhe Li
Department of Computing
Hong Kong Polytechnic University
richie.li@connect.polyu.hk

Man Lung Yiu
Department of Computing
Hong Kong Polytechnic University
csmlyiu@comp.polyu.edu.hk

Tsz Nam Chan
Department of Computer Science
Hong Kong Baptist University
edisonchan@comp.hkbu.edu.hk

***Abstract*—In distributed storage systems (e.g., HDFS, Amazon S3, Databricks), partitioning is applied on a dataset in order to enhance performance and availability. Recently, partitioning methods have been designed to optimize the query performance of partitions with respect to the historical query workload. Nevertheless, in practice, future query workloads may deviate from the historical query workload, thus deteriorating the performance of existing partitioning methods.**

To fill this research gap, we model the variance of future query workloads from the historical query workload, then exploit this characteristic to produce partitions that perform well for future query workloads. In addition, we explore the space of irregular shaped partition regions to further optimize the query performance. Experimental results on TPC-H and real datasets show that our proposal is up to 70× more efficient than the state-of-the-art method.

I. Introduction

In many applications, distributed systems (e.g., Hadoop, Spark) are employed to store and query a vast amount of data. These systems adopt block-based storage (e.g., HDFS, Amazon S3, Databricks), which partitions a dataset into large data blocks[1], then provides access at the block level. During query processing, it suffices to fetch the data blocks whose semantic descriptions intersect with the query region. Recent studies [1]–[5] have used the historical query workload to construct partitions in order to reduce the query cost.

We conceptually visualize three scenarios for partitioning in Figure 1, based on the similarity between the historical query workload and future query workloads. The historical query workload Q_H is denoted by a red dot, whereas future query workloads in different time periods Q_{F1}, Q_{F2}, Q_{F3} are represented by blue dots.

- **The most specific:** The first scenario (Figure 1a) assumes that future workloads have exactly the same distribution as the historical workload. The state-of-the-art solution is the Qd-tree [1], which aims to optimize the performance of partitions with respect to the historical workload only. However, the above assumption is seldom true in practice, causing performance deterioration on future workloads, as we shall discuss shortly.
- **The most generic:** The third scenario (Figure 1c) considers exploratory queries [6]–[9]; future workloads are unpredictable and may vary significantly from the historical workload. The typical solution is to partition the dataset based on data distribution (e.g., k-d tree, R-tree), like in SpatialHadoop [5].

This work was supported by grant GRF 152050/19E from the Hong Kong RGC.

[1]For example, the typical size of a data block in HDFS is 128MB.

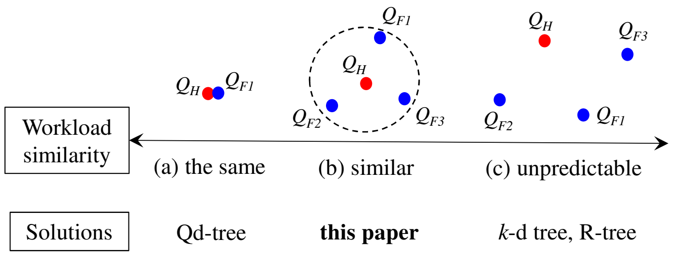

Fig. 1: The similarity between the historical workload Q_H and future workloads Q_{F1}, Q_{F2}, Q_{F3}, in three scenarios

In this paper, we explore the alternative scenario in Figure 1b, where future workloads are similar to the historical workload. Observe that concepts in machine learning (e.g., model, training set, testing set) [10] are analogous to the corresponding concepts in our problem (i.e., partition layout, historical workload, future workload). *Overfitting* occurs when a model is optimized to fit the training set (e.g., Q_H) closely; however, such a model does not *generalize* well to the testing set (e.g., Q_{F1}, Q_{F2}, Q_{F3}).

A. Limitations of existing solutions

Unfortunately, our scenario cannot be efficiently addressed by the solutions from other scenarios. Obviously, the solutions from the third scenario (e.g., k-d tree, R-tree) are inefficient because they do not exploit any workload information.

The best solution from the first scenario suffers from *overfitting* when it is used in our scenario. We exemplify this concern in Figure 2 on a dataset with two attributes A and B. By building the Qd-tree [1] on the historical workload $Q_H = \{q_1, \cdots, q_4\}$, we obtain the partition layout $\mathcal{P} = \{P_1, \cdots, P_5\}$ shown in Figure 2a. The future workload is $Q_F = \{q'_1, \cdots, q'_4\}$, where q'_i is similar to q_i. Although the partition layout $\mathcal{P}$ is efficient for the historical workload, it incurs high cost for the future workload. For instance, the I/O cost for q_1 in Figure 2a is 220MB only; however, the I/O cost for q'_1 in Figure 2b is 790MB because q'_1 intersects all partitions. This phenomenon is similar to the concept of overfitting in machine learning [10].

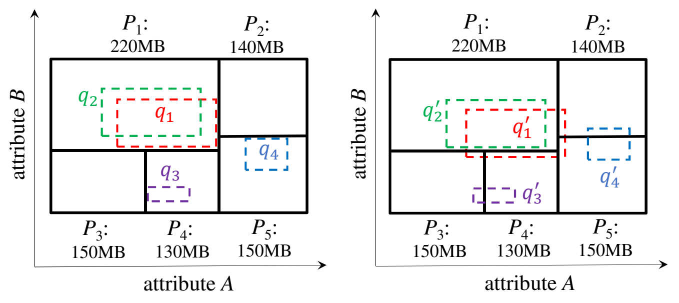

(a) the partition layout generated by Qd-tree on the historical workload

(b) the same partition layout used for a future workload

Fig. 2: An example of historical queries and future queries in workload-aware partitioning

In addition, existing partitioning methods produce rectangular partitions only. Frequently-used partitions (e.g., P_1 in Figure 2a) may cover rarely-queried regions and thus deteriorate the query performance. We demonstrate an alternative partition layout in Figure 3, which contains three rectangular partitions (P_1, P_2, P_3) and an irregular shape partition (P_4). Our idea is to enlarge P_4 (in any shape) as much as possible in order to cover rarely-queried regions, and thus reduce the sizes of more frequently-used partitions (e.g., P_1, P_2, P_3). Observe that the query cost of query q_2 is reduced from 220MB in Figure 2a to 160MB in Figure 3.

TABLE I: Methods for partitioning

✓ Support ▽ No optimization × No support

Method	Qd-tree [1]	*k*-d tree [11]	PAW (ours)
Exact workload (Fig. 1a)	✓	▽	✓
Similar workload (Fig. 1b)	▽	▽	✓
Unpredictable workload (Fig. 1c)	▽	✓	✓
Workload-aware	✓	×	✓
Data-aware	×	✓	✓
Irregular shape partition	×	×	✓

Table I summarizes the properties of methods appeared in Figure 1. Although our solution focuses on the second scenario (Figure 1b), it can also be adapted to the first scenario (Figure 1a) and the third scenario (Figure 1c).

B. Our challenges and contributions

Our key challenges in this paper are as follows. (1) How to generalize the historical workload to future workloads? (2) How to utilize the generalized workload to produce an efficient partition layout? (3) How to exploit irregular shape partitions to boost the query performance?

To tackle the above challenges, we make the following contributions:

- To avoid overfitting, we formulate a data partitioning problem that considers the generalization of the historical workload.
- We propose Partitioning Aware of Workload Variance (PAW), a workload-aware partition technique that is robust to future queries. It exploits irregular shape partitions to reduce the query cost.

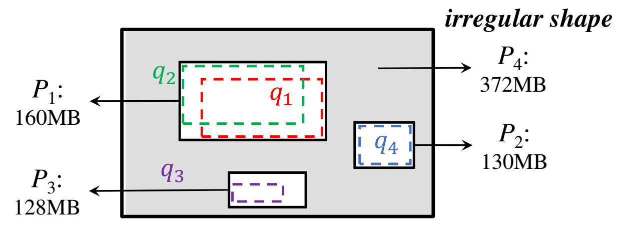

Fig. 3: An example of using irregular shape partitions for historical queries.

- We develop two plugin optimizations to further boost the query performance.
- Extensive experiments are conducted to validate the performance of the proposed methods. PAW outperforms the state-of-the-art method Qd-tree [1] by up to 70×.

The rest of the paper is organized as follows. We first review the related work in Section II. Next, we introduce preliminaries in Section III. Then, we present our PAW partitioning algorithms in Section IV, followed by two plugin optimizations in Section V. Lastly, we present our experiments in Section VI and conclude in Section VII.

II. Related Work

Data partitioning is common in databases and big data processing systems. We first review existing partitioning techniques in Section II-A, then discuss partition pruning in Section II-B.

A. Partitioning

We classify existing partitioning techniques into three categories (i.e., independent, data-aware, and workload-aware).

Independent partitioning assigns records to partitions based on a mapping function that does not rely on the data distribution nor query workloads. Range partitioning and hash partitioning are frequently used in database systems [12], [13], Hive [14], and Spark [15].

Data-driven proposals mainly utilize traditional indexing to generate partition layouts, such as B-tree [16], *k*-d tree [11] and R-tree [17]. For example, SpatialHadoop [5] partitions data according to spatial locality with a R-tree like mechanism. Notice these approaches partition the dataset only according to the data distribution and provide relatively stable performance to queries with different focus. However, these methods are inefficient when the query workloads follow certain distribution.

Workload-aware approaches exploit the workload to produce partition layouts. Auto-tuning and AutoAdmin methods [18]–[24] attempt to find a good physical design of a database according to a given workload. These physical designs include index selection, compression options, update policy, buffering options and partitioning options for data organization. However such methods may take much time (or iteration) in exploring a huge space of parameters. On the contrary, adaptive physical design methods [25]–[27] generate the physical design incrementally and adaptively with periodic update to amortize the exploration cost. However, all these methods generate partitions with simple horizontal or hash split on certain selected dimensions, which again may have poor performance when the query workloads involve many dimensions.

Adaptive partitioning techniques such as AQWA [4] and Amoeba [2] consider the scenario that future workloads shift gradually over time. To be adaptive, they continuously update partitions as future queries arrive (in a streaming manner), which imposes expensive overheads on updating partitions. However, their techniques are not efficient in our scenario where the workloads vary within a limited scope (i.e., the dotted scope in Figure 1b). In our problem setting, there is no need to update the descriptors of partitions, provided that the future workload is sufficiently similar to the historical workload.

Sun et al. [28] formulate the "MaxSkip" partitioning problem and prove it NP-hard. They propose a bottom-up clustering approach which iteratively merges unique binary feature vectors that produce the lowest penalty. The experimental study in [1] has demonstrated that Qd-tree [1] outperforms the solution in [28] by at most 61 times. Note that both [1] and [28] have not dealt with the overfitting problem and our scenario (see Figure 1b).

Some techniques use graph-based workload modeling to generate partition layouts [21], [29], [30]. However, such works are used to optimize the cost caused by mutual network transfer or data shuffling, which differ from our cost target (i.e., minimizing data scan).

Recently, machine learning based methods are getting increasingly popular. SageDB [31] provides a vision of future database which replaces most of its components by machine learning alternatives, including the partition layout generator. Both Yang et al. [1] and Hilprecht et al. [32] provide reinforcement learning agents to find suitable partition layout. However the former has similar performance with its heuristic based alternative and the latter can only produce coarse-grained partitioning (e.g., hash).

Ding et al. [33] leverage sideway information generated from analytic queries with join operations to improve partitioning on multi-table scenarios, which is orthogonal to ours (i.e., single dataset / table partitioning) and could be combined with existing partitioning approaches.

B. *Query Evaluation with Partition Pruning*

Partition pruning has been frequently used to improve query performance. Specifically, one may maintain some aggregate information such as min, max, count and sum for each dimension in each partition, which is known as small materialized aggregates (SMAs) [34]. Then, the SMAs will determine whether a partition contains the query result or not and directly prune the partitions that have no overlap with the given query. Among all the SMAs, the min-max based aggregate is most popular and have been used in various databases like Oracle [35], PostgreSQL [36] and SQLServer [37] to skip irrelevant partitions. Besides these industry databases, many research works [1], [4], [28], [38] also design their algorithms based on partition pruning.

III. Preliminaries

A. *Problem Definition*

In this paper, we consider multi-dimensional range queries on a dataset $\mathcal{D}$ with dimensionality d_{max}. According to [1], [2], SQL queries with unary predicates (in the `WHERE` clause) can be converted to range queries. We shall elaborate the details in Section III-B.

A partition layout $\mathbb{P}$ is a collection of disjoint partitions (say, $P_1, P_2, \cdots, P_n$) so that their union equals to the dataset $\mathcal{D}$. Each partition P_i has a descriptor to indicate the ranges of records stored in P_i.

Many block-based storage systems (e.g., HDFS, Amazon S3, Databricks) impose a minimal size b_{min} on a block (e.g., 128MB in HDFS). We adopt this constraint so that the generated partitions will not be too small. Thus, we require the size of each partition to be at least b_{min}. As a remark, in this paper we only care about logical partitions (i.e., which partition to place for each record). We leave the underlying storage layer to decide the physical placement of blocks and the replication policy.

The I/O cost of a query q on a partition layout $\mathbb{P}$, denoted by $Cost(\mathbb{P}, q)$, is defined as the total size of the partitions in $\mathbb{P}$ that intersect with q. Then, we define the I/O cost of a query workload Q (i.e., a set of queries) on $\mathbb{P}$ by summing the cost of each query in Q.

$$Cost(\mathbb{P}, q) = \sum_{p_i \in \mathbb{P}, p_i \cap q \neq \emptyset} p_i.size \quad (1)$$

$$Cost(\mathbb{P}, Q) = \sum_{q \in Q} \sum_{p_i \in \mathbb{P}, p_i \cap q \neq \emptyset} p_i.size \quad (2)$$

Generalization is the key to address overfitting. Our idea is to generalize the historical workload Q_H into a collection of possible workloads that are sufficiently similar to Q_H. Based on this idea, we formulate the distance between the historical workload Q_H and the future workload Q_F. First, we define the distance between two queries as the maximal difference between them in any dimension. This definition is inspired by the L_∞ norm in the vector space.

Definition 1 (Distance between two queries): The distance between two queries q_i and q_j, denoted by $dist_\square(q_i, q_j)$, is defined as

$$dist_\square(q_i, q_j) = \max_{d=1..d_{max}} \max(|q_i.l_d - q_j.l_d|, |q_i.u_d - q_j.u_d|), \quad (3)$$

where $q_i.l_d$ and $q_i.u_d$ denote the lower and upper values of q_i on the d-th dimension.

Next, we propose the following test on whether two workloads Q_H and Q_F are similar. This definition allows different workload sizes, but requires $|Q_F|$ to be divisible by $|Q_H|$.

Definition 2 (δ-similar workloads): Let δ be a distance threshold. Two workloads Q_H and Q_F are said to be δ-similar if there exists a matching $\mathcal{M} \subset Q_F \times Q_H$ such that: (i) each pair $(q'_i, q_j) \in \mathcal{M}$ satisfies $dist_\square(q'_i, q_j) \leq \delta$ (ii) each $q'_i \in Q_F$

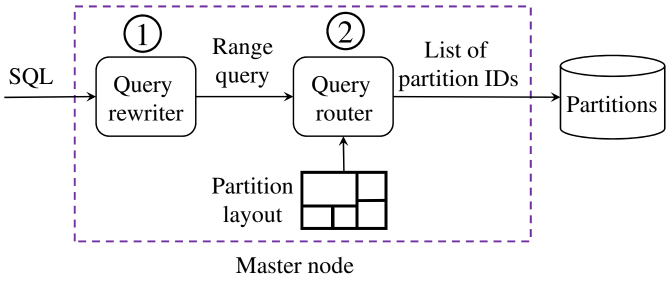

Fig. 4: The query framework of PAW

appears exactly once in $\mathcal{M}$, and (iii) each $q_j \in Q_H$ appears exactly $\frac{|Q_F|}{|Q_H|}$ times in $\mathcal{M}$.

The last condition guarantees that the matching is not dominated by any particular query in Q_H. As a remark, the system parameter δ should be chosen by system administrators. We also provide some heuristics to estimate δ from the historical workload (to be discussed in Section IV-E). We leave for future work the alternative definitions of δ-similar workloads.

We now formally define our problem as follows.

Problem 1 (Partitioning for Worst-Case Future Workload): Given a historical workload Q_H, a dataset $\mathcal{D}$, and a threshold δ, this problem asks for the partition layout $\mathbb{P}$ such that (i) the size of each partition $P_i \in \mathbb{P}$ is at least b_{min}, and (ii) it minimizes the following worst-case cost

$$WCost(\mathbb{P}) = \max_{\delta\text{-similar}(Q_H, Q_F)} \frac{1}{|Q_F|} \cdot Cost(\mathbb{P}, Q_F),$$

for any possible future workload Q_F that is δ-similar to Q_H. The factor $\frac{1}{|Q_F|}$ is used to obtain the average cost per query.

Our problem can address overfitting because it considers a collection of possible workloads. It is also challenging because it involves infinite possible instances of the future workload Q_F.

B. Query Processing

We illustrate the flow of query processing in Figure 4. The master node (of the cluster) manages the meta information of the partition layout in memory (e.g., descriptors and sizes of partitions).

First, when a SQL query is received, the *query rewriter* converts it into one or more range queries. For example, a SQL query with `WHERE A>=10 AND B<=50` corresponds to the range query $[10, \infty) \times (-\infty, 50]$. As another example, a SQL query with `WHERE A>=10 OR B<=50` can be decomposed into two disjoint range queries $[10, \infty) \times (-\infty, \infty)$ and $(-\infty, 10) \times (-\infty, 50]$.

Second, the *query router* examines the partition layout to find the relevant partitions, computes the union list of partition IDs (in case of multiple sub-queries), and then sends the list of partition IDs to the underlying storage system.

IV. Construction of PAW

In this section, we present our techniques to construct the partition layout for Problem 1. First, in Section IV-A, we simplify our partitioning problem but without sacrificing the query cost. Next, we propose split methods in Sections IV-B and IV-C. Then, we summarize our construction algorithm in Section IV-D. Finally, we discuss how to deal with unknown δ in Section IV-E.

A. Reducing the Problem

Recall that, in Problem 1, the equation of $WCost(\mathbb{P})$ involves infinite possible instances of the future workload Q_F. To simplify this problem, we plan to rewrite that equation so that it involves one workload only.

Our idea is to extend each historical query $q_i \in Q_H$ into a new query q_i^* by δ along all directions, i.e.,

$$[q_i^*.l_d, q_i^*.u_d] = [q_i.l_d - \delta, q_i.u_d + \delta]$$

An example is shown in Figure 5.

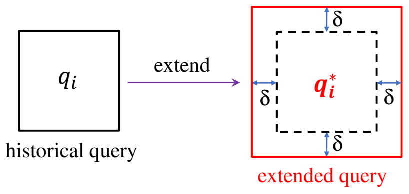

Fig. 5: An example of extended query

Next, we construct the *worst-case workload* Q_F^* as the collection of q_i^*. The following lemma shows that $WCost(\mathbb{P})$ can be expressed by using a single workload (Q_F^*).

Lemma 1: For any partition $\mathbb{P}$, we have:

$$WCost(\mathbb{P}) = \frac{1}{|Q_F^*|} \cdot Cost(\mathbb{P}, Q_F^*)$$

.

Proof: Let Q_F be a workload such that it is ϵ-similar to Q_H. We first consider the case that Q_F and Q_H have the same size, so that we ignore the factor $\frac{1}{|Q_F^*|}$ in the equation of $WCost(\mathbb{P})$.

According to Definition 2, there exists one-to-one matching $\mathcal{M}$ between Q_F and Q_H such that each pair $(q_i', q_j) \in \mathcal{M}$ satisfies $dist_\square(q_i', q_j) \leq \delta$. Without loss of generality, we assume that $q_i \in Q_H$ corresponds to $q_i' \in Q_F$ in the matching $\mathcal{M}$.

Observe that q_i^* (in Q_F^*) contains the maximal query range with respect to $dist_\square(q_i^*, q_i) = \delta$. Thus, we conclude that q_i^* contains q_i'. Next, we get $Cost(\mathbb{P}, Q_F^*) \geq Cost(\mathbb{P}, Q_F)$, and then obtain: $WCost(\mathbb{P}) = Cost(\mathbb{P}, Q_F^*)$.

The above arguments can be generalized to Q_F with other sizes, except that each query in Q_H corresponds to $\frac{|Q_F|}{|Q_H|}$ queries in Q_F. ■

In subsequent sections, we shall use the worst-case workload Q_F^* to build partitions.

B. Partitioning with Irregular Shapes

In this section, we exploit irregular shapes in data partitioning to lower the query cost by reducing the sizes of frequently-queried regions as much as possible.

In subsequent examples, we begin from an initial partition P_o and denote the worst-case workload as $Q_F^* = \{q_1^*, q_2^*, \cdots\}$.

First, we examine an ideal case in which the queries in Q_F^* are mutually disjoint. Figure 6a shows the initial partition P_o and the queries in Q_F^*. Our idea is to divide P_o into four partitions as shown in Figure 6b. P_1, P_2, P_3 can be used to answer q_1^*, q_2^*, q_3^*, respectively. The remaining records are placed in an irregular shape partition (P_4).

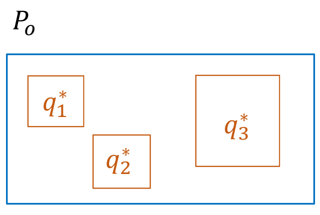

(a) initial partition P_o

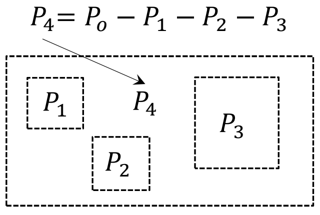

(b) partitions P_1, P_2, P_3, P_4

Fig. 6: Optimal partitions for disjoint queries

Next, we consider a more complicated case in which some queries in Q_F intersect, as shown in Figure 7a. Our idea is to merge intersecting queries (e.g., q_1^*, q_4^*, q_5^*) into a *minimum bounding rectangle* (MBR), then create a grouped partition (e.g., GP_1) for records in that MBR. With this idea, we obtain three grouped partitions (GP_1, GP_2, GP_3) and an irregular partition (IP) in Figure 7b. Recall that our partitioning problem imposes a constraint on the size of each partition (i.e., at least b_{min}). If any partition has a size below b_{min}, then we expand it in order to satisfy the size constraint, like in Figure 7c.

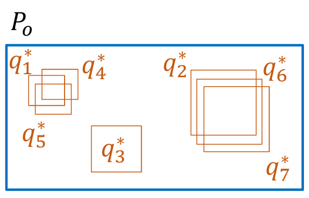

(a) initial partition P_o

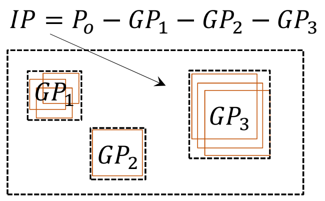

(b) partitions GP_1, GP_2, GP_3, IP

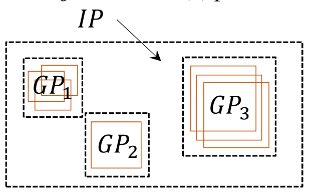

(c) expanded partitions

Fig. 7: Multi-Group Split

We elaborate how to expand a partition in Figure 8. Conceptually, a rectangular region GP can be expressed as $GP.\vec{c} \pm GP.\vec{r}$, where the center vector $GP.\vec{c}$ and the radius vector $GP.\vec{r}$ are defined as follows.

$$GP.\vec{c} = \left[\frac{GP.l_d + GP.u_d}{2}\right]_{d=1..d_{max}}$$

$$GP.\vec{r} = \left[\frac{GP.u_d - GP.l_d}{2}\right]_{d=1..d_{max}}$$

With these concepts, the region GP can be enlarged by a factor f along all dimensions via the following expression.

$$GP' = GP.\vec{c} \pm f \cdot GP.\vec{r}$$

For example, in Figure 8, the region GP' is obtained by enlarging GP with the factor $f = 1.5$.

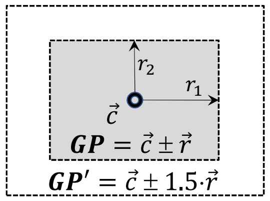
r_2
r_1
$\vec{c}$
$GP = \vec{c} \pm \vec{r}$
$GP' = \vec{c} \pm 1.5 \cdot \vec{r}$

Fig. 8: Expand a partition

Our next step is to find the minimal factor f such that the size of GP' is at least b_{min}. Given a record x, we define its *relative position* in region GP as follows.

$$F_{GP}(x) = \max_{d=1..d_{max}} \frac{|x_d - GP.\vec{c}_d|}{GP.\vec{r}_d}$$

Consider the initial partition P_o in which GP is split from. We sort the records in P_o in the ascending order of $F_{GP}(x)$, then follow this order to assign records to GP until satisfying the size constraint b_{min}.

We summarize our split method in Algorithm 1. At lines 2-4, we create grouped partitions, like in Figure 7b. When the size of a grouped partition GP_i is below b_{min}, we expand it by using the aforementioned idea (at line 5). At line 7, we test whether all grouped partitions are mutually disjoint. If so, then we return them together with an irregular partition IP as the result. Otherwise, an empty result is returned to indicate a failure split.

Algorithm 1 Multi-Group Split

```
     Input: partition $P_o$, workload $Q_F^*$, min block size $b_{min}$
 1:  $\mathbb{P} \leftarrow \emptyset$
 2:  check the intersection relationships of queries in $Q_F^*(P_o)$
 3:  for each group of intersecting queries in $Q_F^*(P_o)$ do
 4:      create a grouped partition $GP_i$
 5:      expand $GP_i$ until $GP_i.size \geq b_{min}$
 6:      insert $GP_i$ to $\mathbb{P}$
 7:  if $\forall GP_i, GP_j \in \mathbb{P}, GP_i \cap GP_j = \emptyset$ then
 8:      $IP \leftarrow P_o - \bigcup_{GP_i \in \mathbb{P}} GP_i$
 9:      if $IP.size \geq b_{min}$ then
10:          return $\mathbb{P} \cup \{IP\}$
11:  return $\emptyset$
```

C. Rectangular Split

In some cases, rectangular partitions may perform better than irregular partitions. Therefore, we introduce this complementary query-driven partition technique. To illustrate this, we consider the example in Figure 9, where the minimum block size b_{min} is 128 MB. Observe that q_1^* and q_2^* have partial intersection, so the MBR of these two queries is huge.

Applying the method in Section IV-B on this example, the solution degenerates into a single partition P, as shown in

Figure 9a. The query cost can be reduced to 465MB if we divide P into two irregular partitions as shown in Figure 9b. Interestingly, if we employ only rectangular partitions like in Figure 9c, the query cost can be further reduced to 420MB.

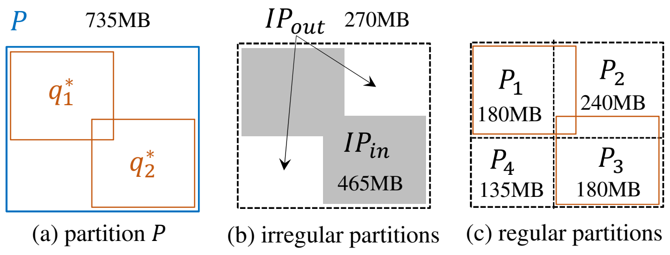

Fig. 9: A case where rectangular partitions perform better

As such, we also consider existing query-driven partitioning methods that are axis-parallel and produce rectangular partitions. Specifically, for each dimension d, we consider a possible split at (i) the median of P in this dimension, and (ii) the lower and upper values of each query in $Q_F^*(P)$. Observe that (ii) has also been used in the Qd-tree [1].

We summarize this split method in Algorithm 2.

Algorithm 2 Axis-Parallel Split

```
    Input: partition $P$, workload $Q_F^*$, min block size $b_{min}$
1:  let $\mathcal{APS}$ be the set of axis-parallel splits
2:  $\mathbb{P}_{best} \leftarrow \emptyset$; $cost_{best} \leftarrow \infty$
3:  for $split_i$ in $\mathcal{APS}$ do
4:      $\mathbb{P}' \leftarrow$ divide $P$ by using $split_i$
5:      if $\forall p_i \in \mathbb{P}'$, $p_i.size \geq b_{min}$ then
6:          if $cost_{best} > Cost(\mathbb{P}', Q_F^*(P))$ then
7:              $\mathbb{P}_{best} \leftarrow \mathbb{P}'$; $cost_{best} \leftarrow Cost(\mathbb{P}', Q_F^*(P))$
8:  return $\mathbb{P}_{best}$
```

D. The Construction Algorithm

We propose a recursive algorithm to construct partitions (see Algorithm 3). Its parameters include: (i) the initial partition P_o, (ii) the worst-case workload Q_F^* as described in Section IV-A, and (iii) the split policy Ψ which will be discussed later. In the root recursive call, P_o is initialized to the MBR of the dataset $\mathcal{D}$. In lines 1-6, we apply each split function SF_i on the initial partition P_o, measure the cost of the resulting partition layout $\mathbb{P}'$, and update the best layout $\mathbb{P}_{best}$ when $\mathbb{P}'$ yields a lower cost. If $\mathbb{P}_{best}$ is better than P_o, then we replace P_o by $\mathbb{P}_{best}$ and invoke a recursive call on each partition in $\mathbb{P}_{best}$. However if P_i is irregular shape, the partitioning process terminates once it is generated as an irregular shape partition contains no queries in Q_F^* and no splits could reduce its cost if it is already 0.

Note that, at line 2, the split policy Ψ is used to decides the list of applicable split methods for P_o. Ideally, both irregular split (Alg. 1) and rectangular split (Alg. 2) should be tried at line 2, in order to optimize the query cost. However, Alg. 1 is time-consuming and it is effective on small to medium sized partitions. To control the trade-off between the quality and construction time, we recommend to use the following split policy Ψ:

$$\Psi(P_o) = \begin{cases} \{\text{Alg. 1}, \text{Alg. 2}\}, & \text{if } P_o.size \geq \alpha \cdot b_{min} \\ \{\text{Alg. 2}\} & \text{if } P_o.size \geq 2 \cdot b_{min} \\ \emptyset & \text{otherwise} \end{cases} \quad (4)$$

where α is a constant larger than 1. We shall test the effect of α in our experimental study.

Algorithm 3 PAW-Construction

```
    Input: the initial partition $P_o$, the worst-case workload $Q_F^*$, the
    split policy $\Psi$
1:  $\mathbb{P}_{best} \leftarrow \emptyset$; $cost_{best} \leftarrow \infty$
2:  for $SF_i$ in $\Psi(P_o)$ do
3:      $\mathbb{P}' \leftarrow SF_i(P_o)$
4:      if $\mathbb{P}' \neq \emptyset$ then
5:          if $Cost(\mathbb{P}', Q_F^*(P_o)) < cost_{best}$ then
6:              $\mathbb{P}_{best} \leftarrow \mathbb{P}'$; $cost_{best} \leftarrow Cost(\mathbb{P}', Q_F^*(P_o))$
7:  if $cost_{best} < Cost(P_o, Q_F^*(P_o))$ then
8:      for $P_i$ in $\mathbb{P}_{best}$ do
9:          add $P_i$ as a child of $P_o$
10:         PAW-Construction$(P_i, Q_F^*, \Psi)$
```

Figure 10 demonstrates some running steps of our construction algorithm. The relationships between different recursive calls (and partitions) can be visualized as the *partition tree*, in Figure 10d. The leaf nodes correspond to the final partitions P_A, P_B, P_C, P_D in the storage system. The partitions for non-leaf nodes are not stored physically; instead, we only maintain their descriptors in the master node in order to facilitate query routing.

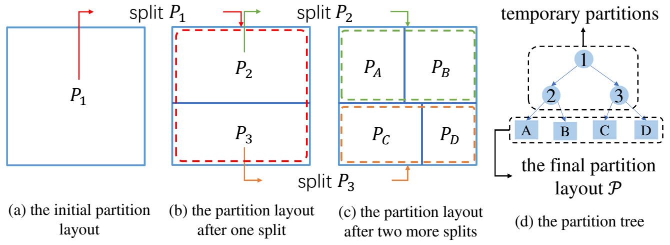
split P_1
split P_2
split P_3
P_1
P_2
P_3
P_A
P_B
P_C
P_D
temporary partitions
1
2
3
A
B
C
D
the final partition layout $\mathcal{P}$
(a) the initial partition layout
(b) the partition layout after one split
(c) the partition layout after two more splits
(d) the partition tree

Fig. 10: Example of PAW construction

As a remark, Algorithm 3 is a greedy heuristics algorithm; it makes locally optimal choices but does not guarantee the globally optimal solution. Alternative search strategies (e.g., beam search [39]) may be applied to broaden the search space and revise Algorithm 3. We leave this issue for future work.

E. Dealing with Unknown δ

In real applications, the distance threshold δ can be unknown. We propose a simple heuristics to estimate the threshold by using the historical workload Q_H. First, we simulate the past and future by dividing Q_H equally into two workloads Q_{H1} and Q_{H2}, according to their timestamps in the system. Next, we compute the minimal value (say, δ') such that Q_{H1} and Q_{H2} are δ'-similar (see Definition 2). Then, we use δ' as the distance threshold.

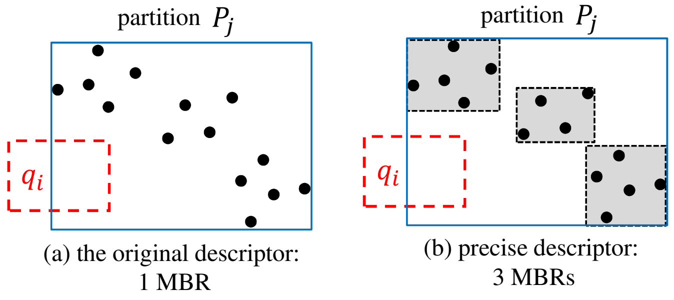
partition P_j
q_i
(a) the original descriptor: 1 MBR
partition P_j
q_i
(b) precise descriptor: 3 MBRs

Fig. 11: Descriptors for a partition P_j

Note that Algorithm 3 stops partitioning when a region does not intersect with any query in Q_F^*. Some partitions can be huge and may cause performance deterioration if some future queries partially intersect with them. This happens when the estimated δ' is less than the real δ. To alleviate this issue, we keep split the leaves of a partition tree by data-aware partitioning (e.g., k-d tree partitioning) until reaching the finest size (i.e., $[b_{min}, 2b_{min})$).

V. Plugin Modules

We shall present two plugin modules to boost the query performance, after constructing the partition layout. They are orthogonal to the techniques proposed in Section IV.

A. The Precise Descriptor Module

This module represents partitions by using more precise descriptors in order to enhance the pruning power during query processing.

As an example, consider the partition P_j in Figure 11, where black dots denote the actual records stored in P_j. We compare the original descriptor of P_j (in Figure 11a) and the precise descriptor of P_j (in Figure 11b), by using the query q_i. The original descriptor of P_j is just the MBR of P_j, which intersects with the query q_i. Thus, we still need to scan the data stored in P_j. In Figure 11b, we use a more precise descriptor of P_j, i.e., a set of 3 gray MBRs that collectively cover all records in P_j. Since q_i does not intersect with any gray MBR, we avoid scanning the data stored in P_j.

Existing data partitioning algorithms may be used to construct the above precise descriptor. In our implementation, we adopt the R-tree construction algorithm to extract a given number of MBRs (say N_{mbr}) from a partition. Like the partition layout, the precise descriptors of partitions are stored in the memory in the master node (cf. Figure 4) . During query processing, the master node checks whether a query (say q_i) intersects with any MBR in the precise descriptor of partition P_j. If there is no intersection, we skip the scanning of P_j.

As a remark, a precise descriptor occupies only $16 \cdot d_{max} \cdot N_{mbr}$ bytes, where N_{mbr} is the number of MBRs in the precise descriptor, and d_{max} is the number of dimensions. The extra memory required is very small compared to the size of a partition (e.g., 128MB).

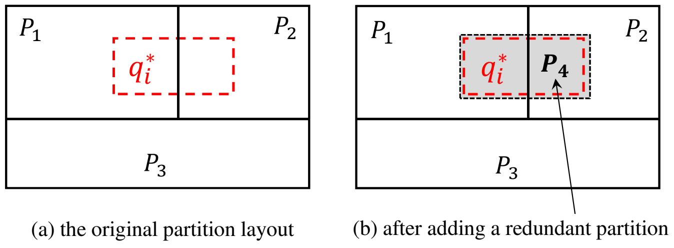
P_1
P_2
q_i^*
P_3
(a) the original partition layout
P_1
P_2
q_i^*
P_4
P_3
(b) after adding a redundant partition

Fig. 12: Plugin redundant partition

B. The Storage Tuner Module

This module exploits the available storage space to construct extra partitions in order to reduce the query cost. Obviously, these extra partitions overlap with some partitions in the original partition layout $\mathbb{P}$.

We proceed to illustrate our idea. In Figure 12a, the original partition layout contains three partitions P_1, P_2, P_3. A query $q_i^* \in Q_F^*$ intersects with both P_1 and P_2. Thus, the I/O cost of q_i^* is $P_1.size + P_2.size$. In Figure 12b, suppose that the gray partition P_4 is included as an extra partition. Note that P_4 can be used to answer q_i^* at a lower cost.

Next, we elaborate how to construct extra partitions, subject to the available storage space. For each query q_j^* in the worst-case workload Q_F^*, we define its extra partition RP_j as the result size of q_j^*. Then, the gain of RP_j is defined as follows.

$$Gain(RP_j) = \frac{\sum_{q_i^* \in Q_F^*, q_i^* \subseteq RP_j} (Cost(\mathbb{P}, q_i^*) - RP_j.size)}{RP_j.size} \tag{5}$$

We implement a greedy algorithm to select extra partitions in descending order of $Gain(RP_j)$, until occupying all the available storage space. When a partition RP_j is selected, we include it into P and update the gain of any other extra partition.

At the query time, the master node first checks whether the query lies within some extra partitions. If yes, then we consult the corresponding extra partition. Otherwise, the query is processed with the original PAW partition layout.

VI. Experimental Evaluation

We conduct extensive experiments to evaluate the performance of PAW. Our key findings are highlighted as follows:

- PAW incurs much lower I/O cost than Qd-tree (2× to 70× better).
- The I/O cost of PAW is only within 1.5× of the theoretical lower bound cost in most of the tested cases.

A. Experimental Setting

Platform. Experiments are conducted on a 4-node Spark cluster connected by LAN. Each node has 8 vCPUs (Intel Skylake, 2.6GHz), 16GB RAM, and 1TB HDD. All data is stored in the Parquet file format in HDFS. For each method, we measure the average end-to-end response time (per query) and the average I/O cost (per query).

Methods. We compare our proposed method PAW with two existing methods: Qd-tree [1] and k-d tree [11]. For PAW, we disable our plugin modules in Section V by default. For Qd-tree [1], we implement its greedy version because it is deterministic and yields comparable performance (to the reinforcement learning variant) in our experiments. For k-d tree [11], we implement the standard version which chooses split dimensions by round-robin and splits from the median. In addition, we also compare with the theoretical lower bound cost, denoted by LBCost, which scans exactly the query result.

Datasets. The TPC-H benchmark[2], with scale factor, is used to generate the `lineitem` table. This table contains 600 million records (75GB) and 8 numerical attributes. We observe that the generated records are uniformly distributed.

We also use a real dataset OSM [40], which contains 100 million records and 2 numerical attributes (latitude and longitude). The records in this dataset follow a skewed distribution.

Following Qd-tree [1], we use a sampled subset (fixed to 6M rows from the dataset) to generate the logical partition layout, then route the full dataset to its corresponding partitions and write each partition to disk. In Table II, we show the breakdown of construction time for 3 different TPC-H dataset sizes (i.e., 8GB, 38GB, and 75GB). The logical partition layout could be generated quickly due to sampling, while routing (i.e., distribute records to partitions) and I/O dominate 90%–99% of the construction time. Therefore, all methods have similar construction time on the same dataset size. It takes approximately 2.4 hours and 0.2 hours to construct partitions on TPC-H (75GB) and OSM, respectively.

TABLE II: Partition construction time for the TPC-H dataset with 3 sizes (8 GB, 38GB, and 75GB)

Methods	Layout generation time (s)	Routing and I/O time (s)		
		8GB	38GB	75GB
Qd-tree	8.68	730	3794	7899
k-d tree	3.43	754	3594	8703
PAW	22.09	737	3880	8769

Query workloads. Following the literature [4], [5], [20], [22], [29], we implement the following two generators to produce the historical workload Q_H. The uniform generator generates historical queries according to the data domain. The skewed generator picks a fixed number of centers and then generates historical queries by the Gaussian mixture model.

The future workload Q_F is generated randomly within a given distance threshold from Q_H. By default, we use a total of 100 queries; 50% in Q_H and 50% in Q_F. The parameters for generating the above workloads are shown in Table III.

B. A Case Study on Partition Layouts

Before diving into detailed comparisons, we visualize the partition layouts generated by different methods. For the sake of visualization, we plot Figures 13 and 14 in the 2-dimensional space. Partition boundaries are shown as green lines, whereas query regions are drawn as red boxes.

[2]http://www.tpc.org/tpch/

TABLE III: Default query properties

Property	Default value
Common workload generator properties	
#Q: the number of queries	100
#dims: the number of dimensions in queries	4
δ: the distance threshold	1% of domain length
γ: the maximal query range	10% of domain length
Skewed workload generator properties	
#C: the number of query centers	10
σ: the standard deviation	10% of γ

For k-d tree, the historical workload (Figure 13a) and the future workload (Figure 14a) have similar query cost. The reason is because each partition has been split to its minimum size (i.e., $[b_{min}, 2b_{min})$). However, a query may partially intersect some partitions and waste I/O cost on scanning records that are not in the query result.

Qd-tree produces the partitions based on the borders of historical queries (see Figure 13b). This could optimize the query cost with respect to the historical workload. However, slightly different future queries may deteriorate the query cost significantly (see Figure 14b).

PAW extends historical queries and applies multi-group splits. Thus, it produces just the right partitions to tolerate variances in the future workload. Each future query is highly likely to fall into a single partition in Figure 14c.

C. Scalability on TPC-H

In Figure 15, we vary the data size of TPC-H, then plot the average I/O cost (per query) and the average end-to-end query response time (per query). in the Spark cluster. PAW outperforms Qd-tree by $10\times$.

Observe that, when the I/O cost is extremely high, the end-to-end query response time grows sub-linearly. This is attributed to the optimizations implemented in the underlying system (e.g., row group based pruning [41], caching). These optimizations (and engineering tricks) are orthogonal to our problem. In subsequent experiments, we measure the I/O cost only because it is platform independent.

D. Robustness to Various Parameters

In this subsection, we measure the *scan ratio* as the ratio of the average I/O cost to the dataset size.

The effect of the number of query dimensions. In Figure 16, we vary the number of dimensions used in queries, by selecting the first few attributes (from the lineitem table in TPC-H) except the primary key. Note that partitions store all the dimensions of records. The I/O cost of PAW is within $1.5\times$ of the theoretical lower bound cost in all tested cases. Qd-tree incurs the highest I/O cost because the future workload deviates from the historical workload and Qd-tree partitions are more likely to have partial intersections with the future workload. When the number of query dimensions increases, the query selectivity drops and thus all methods yield lower I/O cost in general. The spike in the I/O cost of k-d tree, from 2 to 3 query dimensions, happens because k-d tree chooses split

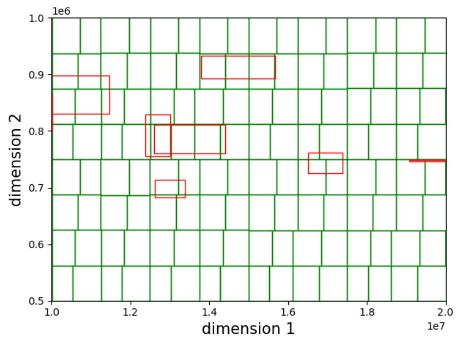

(a) k-d tree on Q_H

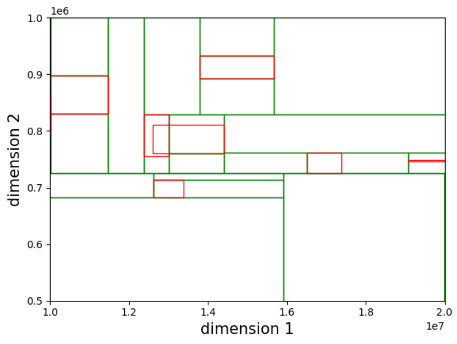

(b) Qd-tree on Q_H

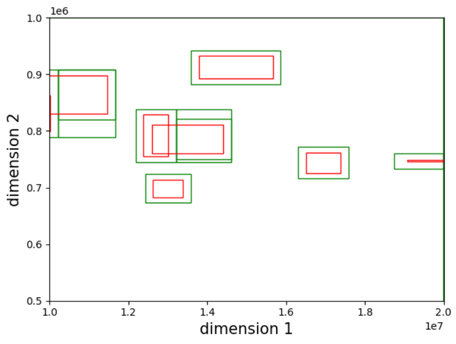

(c) PAW on Q_H

Fig. 13: The historical workload and the partition layout of all methods, on TPC-H

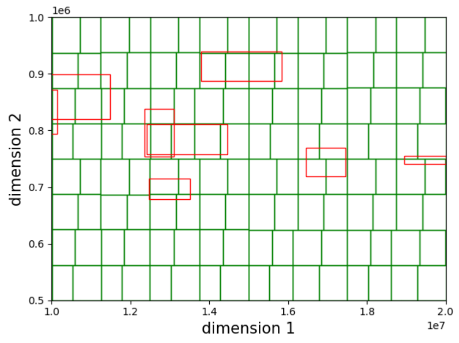

(a) k-d tree on Q_F

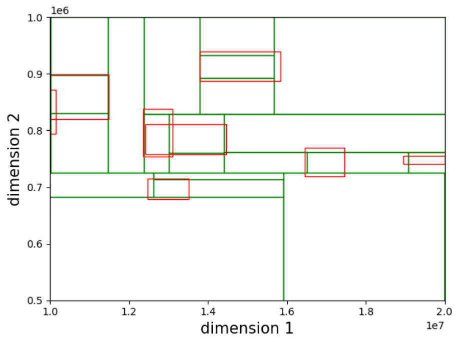

(b) Qd-tree on Q_F

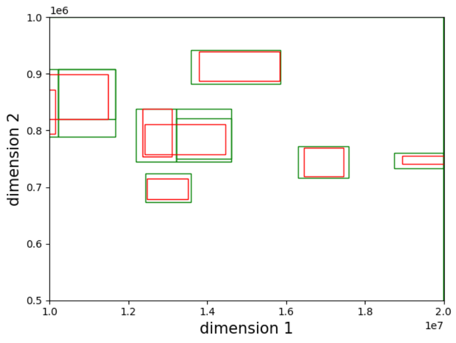

(c) PAW on Q_F

Fig. 14: The future workload and the partition layout of all methods, on TPC-H

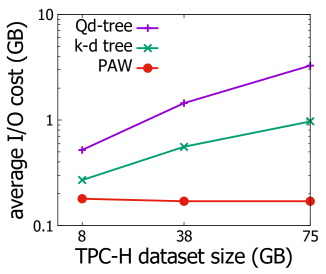

(a) I/O cost

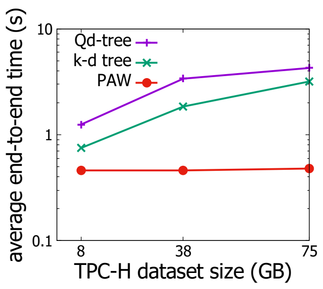

(b) End-to-end time

Fig. 15: Average I/O cost and end-to-end time, on TPC-H

dimensions by round-robin and the 3rd chosen split dimension has a much smaller domain than other attributes.

The effect of the query range. In Figure 17, we vary the maximal query range. As expected, most of the methods incur higher I/O cost as query range increases. Even when the query range is small, the queries in the future query workload may partially intersect large partitions in Qd-tree, as we have demonstrated in Figure 14b. This phenomenon renders the I/O cost of Qd-tree unnecessary high. PAW remains the best method.

The effect of workload size. In Figure 18, we vary the historical workload size. PAW and k-d tree are not very sensitive to this parameter. The I/O cost of PAW is close to the theoretical lower bound cost. In contrast, Qd-tree behaves differently on different data distributions. For a uniform dataset (i.e., TPC-H), a larger historical workload size implies more partitions in Qd-tree, thus leading to more saving in the I/O cost. For a skewed dataset (i.e., OSM), Qd-tree may compute a pathological layout as shown in Figure 14b, where future queries are likely to intersect with multiple partitions. When the number of historical queries is extremely high, the scan ratio of Qd-tree is close to PAW due to the large number of partitions.

PAW outperforms Qd-tree by 70× on TPC-H and 10× on OSM.

The effect of the distance threshold. In Figure 19, we vary the distance threshold δ between the historical workload and the future workload. As expected, a larger δ implies a higher I/O cost. Again, PAW is the best method and its I/O cost is close to the theoretical lower bound cost in most of the cases. Note that a larger δ could also widen the average query range of future queries, leading to a higher scan ratio of all methods.

The effect of the workload distribution. As shown in Figure 20, the I/O cost of most methods rise slowly when we change from the uniform workload to the skewed workload.

For a skewed workload, queries are more likely to have overlapping ranges, rendering it harder to generate efficient partition layouts. The I/O cost of *k*-d tree remains stable because its partition layout does not rely on the historical workload.

The effect of skewed workload parameters. Next, we test the effect of skewed workload parameters: (i) the number of query centers, and (ii) the standard deviation of query range. In Figure 21a, when the number of query centers rises, the I/O cost begins to drop because more partitions will be produced. However, when the number of query centers becomes too high (e.g., 50), overlapping occurs among many queries, thus leading to higher query cost. Note that PAW is not sensitive to this parameter. Figure 21b plots the I/O cost of methods while varying the standard deviation of the query range. PAW performs the best and it is the least sensitive to this parameter.

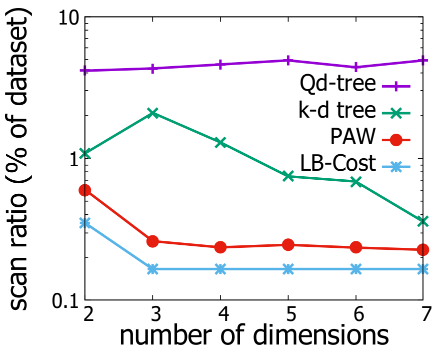

Fig. 16: Average I/O cost on TPC-H, varying the number of query dimensions

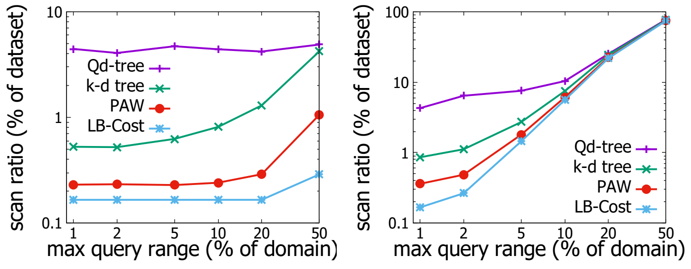

(a) TPC-H (b) OSM

Fig. 17: Average I/O cost on two datasets, varying the maximal query range

E. *The Effect of Unknown Distance Threshold*

We proceed to compare two variants of PAW: (i) PAW, which is given the (real) distance threshold δ, (ii) PAW-unknown, which estimates δ from the historical workload according to Section IV-E. Figure 22a shows the I/O of these two variants of PAW, as well as the theoretical lower bound cost. For uniform workloads, PAW-unknown is worser than PAW by 3 to 4×; nevertheless, the scan ratio (per query) is

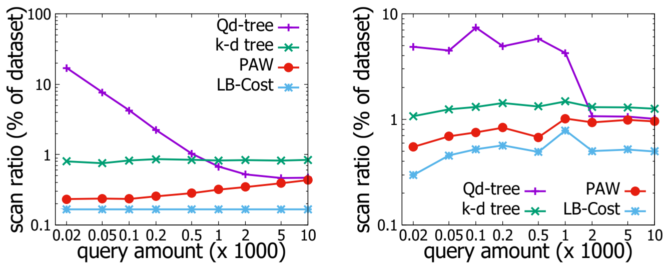

(a) TPC-H (b) OSM

Fig. 18: Average I/O cost on two datasets, varying the number of queries

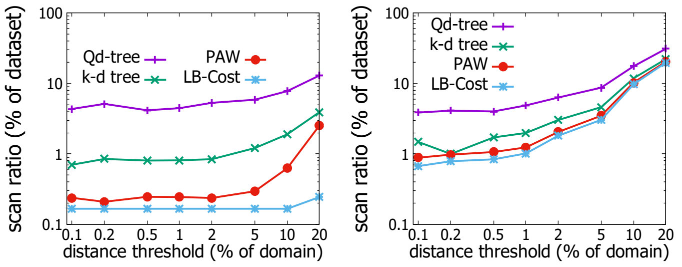

(a) TPC-H (b) OSM

Fig. 19: Average I/O cost on two datasets, varying the distance threshold δ

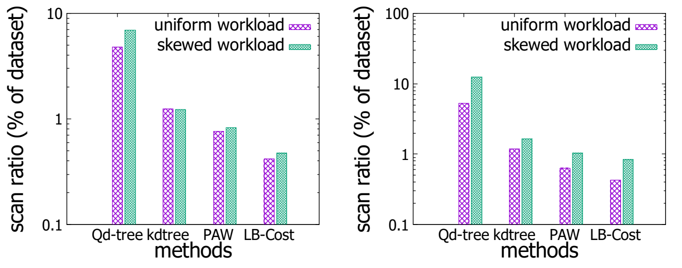

(a) TPC-H (b) OSM

Fig. 20: Average I/O cost on two datasets, varying the distribution of queries

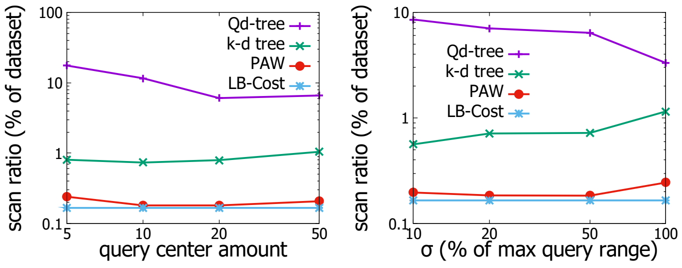

(a) varying #C (b) varying σ

Fig. 21: Average I/O cost on TPC-H, varying the parameters in skewed workload

still below 1% of the entire dataset. For skewed workloads, the performance of PAW-unknown is comparable to PAW.

In the next experiment, we simulate the unpredictable scenario (in Figure 1c) by replacing X% of queries in the future workload with random queries. The historical workload is uniformly distributed. We turn on the data-aware optimization (as discussed in Section IV-E) for PAW. In Figure 22b, we vary the percentage of random queries (in the future workload). Observe that the performance of PAW degrades gracefully from 0% to 100%. In the worst case (i.e., 100% of random), PAW is comparable to a k-d tree. Thanks to the data-aware optimization in Section IV-E, PAW can support the unpredictable scenario shown in Figure 1c.

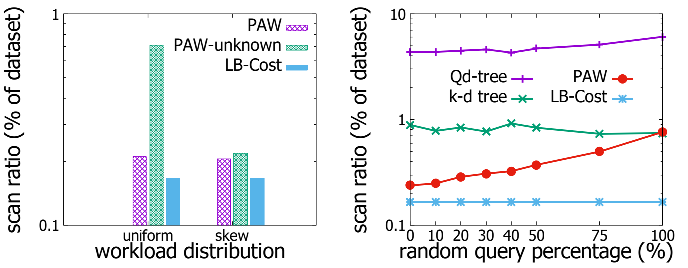

(a) unknown threshold (b) mixing with random queries

Fig. 22: Average I/O cost on TPC-H dataset, using the techniques in Section IV-E

F. Experiments on Plugin Modules

In this subsection, we test the plugin modules described in Section V.

First, we enable the precise descriptor plugin in PAW and vary the number of MBRs per precise descriptor. According to Figure 23a, 3 MBRs per precise descriptor would be sufficient to reduce the query I/O cost by 10%.

Second, we enable the storage tuner plugin in PAW and vary the amount of disk space for storing redundant partitions. According to Figure 23b, when we have 20% more extra space, the query I/O cost of PAW drops by 10%.

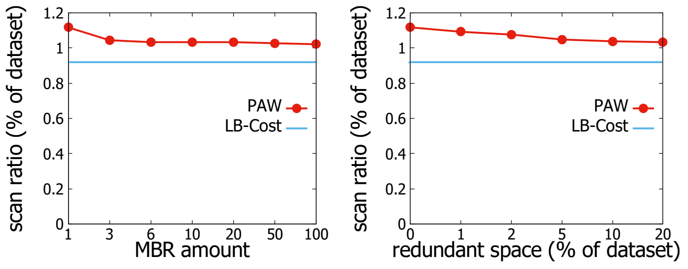

(a) precise descriptor plugin (b) storage tuner plugin

Fig. 23: Average I/O cost on OSM, using plugin modules

G. Experiments on the Special Case $\delta = 0$

In this subsection, we consider the special case $\delta = 0$, which corresponds to the 'same workload' scenario in Figure 1a. This is also the scenario where Qd-tree is designed for.

Even in this special case, PAW still outperforms Qd-tree because we exploit irregular shape partitions (in Multi-Group Split). We rerun our experiments on this setting.

Table IV gives the I/O cost and end-to-end time in Spark cluster when $\delta = 0$ under the default setting. Observe that PAW is 6× more efficient than k-d tree and 1.2× more efficient than Qd-tree.

TABLE IV: Query cost on default settings when $\delta = 0$

Scenario	Measure	k-d tree	Qd-tree	PAW
$\delta = 0$	I/O cost (GB)	0.81	0.18	0.15
$\lvert\mathcal{D}\rvert = 75GB$	end-to-end time (s)	3.11	0.63	0.50

In Figure 24a, we vary the number of query dimensions. Similar to the case when $\delta \neq 0$, the query cost of all methods decrease, which correspond to the selectivity of queries. In Figure 24b, we vary maximum query range. As expected, all methods increase the cost as query range increases. In Figure 24c, we vary number of historical queries. k-d tree is still insensitive to this parameter. When there are many queries, the query distribution becomes more similar to the uniform distribution. Thus, the I/O costs of both Qd-tree and PAW increase as the number of queries increases. In Figure 24d, we test the effect of different query distributions. The result is similar to the $\delta \neq 0$ case.

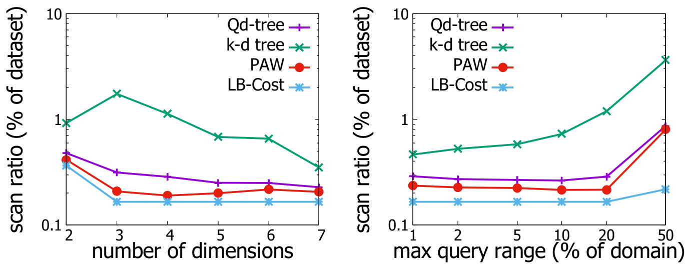

(a) varying #dims (b) varying γ

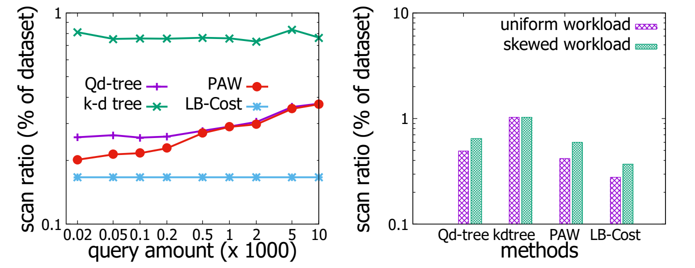

(c) varying $\#Q$ (d) varying distribution

Fig. 24: Average I/O cost on TPC-H dataset, varying query parameters, fixing $\delta = 0$

In Figure 25, we rerun the plugin optimizations. For precise descriptor plugin (Figure 25a), its performance is similar to the case when $\delta \neq 0$ (i.e., Figure 23a). For storage tuner plugin, since now the extra partitions are generated using Q_F^* equivalently ($Q_F^* = Q_H$ when $\delta = 0$), the plugin keep reducing the cost for all method with increasing redundant space until the lower bound is met. Notice under the above two plugin optimizations, PAW still achieves the lowest cost and is close to the theoretical lower bound in all cases.

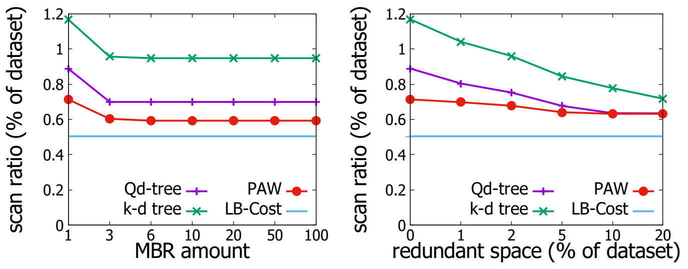

(a) precise descriptor plugin (b) storage tuner plugin

Fig. 25: Average I/O cost on OSM, using plugin modules, fixing $\delta = 0$

VII. Conclusion

In this paper, we study the workload-aware partitioning problem that aims at reducing the query cost for any unknown future workload Q_F. Although existing works assume Q_F are exactly the same as the historical workload Q_H, we allow them to be slightly different (within a distance threshold). We formally define such concept δ-similar workload and show that the worst case query cost is achieved when $Q_F = Q_F^*$, which could be derived from the historical queries Q_H. Our proposed partitioning based on Q_F^* allows us to avoid overfitting, causing the future workload to intersect with fewer partitions in PAW than in the Qd-tree (see Figure 14).

In order to further reduce the query cost on Q_F^*, we propose the Multi-Group Split partition methods to maximize the pruning of non-queried regions, which is also the first partition method that exploits irregular shape partitions and non-axis parallel splits. We combine Multi-Group Split with existing split methods to form a general partition framework PAW. Our experiment results show that PAW could be 10X faster than the state-of-the-art method in query response time in default settings and up to 70X more efficient in certain workload conditions.

In the future, we could have the following explore directions. (1) Algorithms 1 and 2 are based on range queries. How to support more SQL and analytic query operations (e.g., KNN) that could benefit from partitioning? (2) Other than the I/O cost, how to take the storage layer's data placement and network latency issues into one cost model and generate partitions according to it? (3) When more split functions are considered, how to automatically determine their apply conditions?

References

[1] Z. Yang, B. Chandramouli, C. Wang, J. Gehrke, Y. Li, U. F. Minhas, P. Larson, D. Kossmann, and R. Acharya, "Qd-tree: Learning data layouts for big data analytics," in *SIGMOD*, 2020, pp. 193–208.
[2] A. Shanbhag, A. Jindal, S. Madden, J. Quiané-Ruiz, and A. J. Elmore, "A robust partitioning scheme for ad-hoc query workloads," in *SoCC*, 2017, pp. 229–241.
[3] A. M. Aly, H. Elmeleegy, Y. Qi, and W. G. Aref, "Kangaroo: Workload-aware processing of range data and range queries in hadoop," in *Proceedings of the Ninth ACM International Conference on Web Search and Data Mining*, 2016, pp. 397–406.
[4] A. M. Aly, A. R. Mahmood, M. S. Hassan, W. G. Aref, M. Ouzzani, H. Elmeleegy, and T. Qadah, "AQWA: adaptive query-workload-aware partitioning of big spatial data," *PVLDB*, vol. 8, no. 13, pp. 2062–2073, 2015.
[5] A. Eldawy and M. F. Mokbel, "Spatialhadoop: A mapreduce framework for spatial data," in *ICDE*, 2015, pp. 1352–1363.
[6] A. Bozzon, M. Brambilla, S. Ceri, and D. Mazza, "Exploratory search framework for web data sources," *VLDB J.*, vol. 22, no. 5, pp. 641–663, 2013.
[7] M. Singh, M. J. Cafarella, and H. V. Jagadish, "Dbexplorer: Exploratory search in databases," in *EDBT*, 2016, pp. 89–100.
[8] B. Qarabaqi and M. Riedewald, "Merlin: Exploratory analysis with imprecise queries," *IEEE TKDE*, vol. 28, no. 2, pp. 342–355, 2016.
[9] O. B. El, T. Milo, and A. Somech, "Automatically generating data exploration sessions using deep reinforcement learning," in *SIGMOD*, 2020, pp. 1527–1537.
[10] I. Goodfellow, Y. Bengio, and A. Courville, *Deep Learning*. MIT Press, 2016, http://www.deeplearningbook.org.
[11] J. L. Bentley, "Multidimensional binary search trees used for associative searching," *Commun. ACM*, vol. 18, no. 9, pp. 509–517, 1975.
[12] IBM, "Multidimensional clustering tables," https://www.ibm.com/support/producthub/db2/docs/content/SSEPGG_-11.5.0/com.ibm.db2.luw.admin.partition.doc/doc/c0021560.html.
[13] MySQL, "Subpartitioning," https://dev.mysql.com/doc/mysql-partitioning-excerpt/8.0/en/partitioning-subpartitions.html.
[14] Hive, https://hive.apache.org/.
[15] Spark, "Parquet Files," https://spark.apache.org/docs/latest/sql-data-sources-parquet.html.
[16] D. Comer, "The ubiquitous b-tree," *ACM Comput. Surv.*, vol. 11, no. 2, pp. 121–137, 1979.
[17] A. Guttman, "R-trees: A dynamic index structure for spatial searching," in *SIGMOD*, 1984, pp. 47–57.
[18] S. Agrawal, N. Bruno, S. Chaudhuri, and V. R. Narasayya, "Autoadmin: Self-tuning database systems technology." *IEEE Data Eng. Bull.*, vol. 29, no. 3, pp. 7–15, 2006.
[19] J. Rao, C. Zhang, N. Megiddo, and G. M. Lohman, "Automating physical database design in a parallel database," in *SIGMOD*, 2002, pp. 558–569.
[20] M. Olma, M. Karpathiotakis, I. Alagiannis, M. Athanassoulis, and A. Ailamaki, "Slalom: Coasting through raw data via adaptive partitioning and indexing," *PVLDB*, vol. 10, no. 10, pp. 1106–1117, 2017.
[21] A. Pavlo, C. Curino, and S. B. Zdonik, "Skew-aware automatic database partitioning in shared-nothing, parallel OLTP systems," in *SIGMOD*, 2012, pp. 61–72.
[22] E. Wu and S. Madden, "Partitioning techniques for fine-grained indexing," in *ICDE*, 2011, pp. 1127–1138.
[23] S. Agrawal, V. R. Narasayya, and B. Yang, "Integrating vertical and horizontal partitioning into automated physical database design," in *SIGMOD*, 2004, pp. 359–370.
[24] M. Athanassoulis, K. S. Bøgh, and S. Idreos, "Optimal column layout for hybrid workloads," *PVLDB*, vol. 12, no. 13, pp. 2393–2407, 2019.
[25] S. Idreos, M. L. Kersten, and S. Manegold, "Database cracking," in *CIDR*, 2007, pp. 68–78.
[26] F. Halim, S. Idreos, P. Karras, and R. H. C. Yap, "Stochastic database cracking: Towards robust adaptive indexing in main-memory column-stores," *PVLDB*, vol. 5, no. 6, pp. 502–513, 2012.
[27] N. Bruno and S. Chaudhuri, "An online approach to physical design tuning," in *ICDE*, 2007, pp. 826–835.
[28] L. Sun, M. J. Franklin, S. Krishnan, and R. S. Xin, "Fine-grained partitioning for aggressive data skipping," in *SIGMOD*, 2014, pp. 1115–1126.

[29] C. Curino, Y. Zhang, E. P. C. Jones, and S. Madden, “Schism: a workload-driven approach to database replication and partitioning,” *PVLDB*, vol. 3, no. 1, pp. 48–57, 2010.

[30] J. Zhou, N. Bruno, and W. Lin, “Advanced partitioning techniques for massively distributed computation,” in *SIGMOD*, 2012, pp. 13–24.

[31] T. Kraska, M. Alizadeh, A. Beutel, E. H. Chi, A. Kristo, G. Leclerc, S. Madden, H. Mao, and V. Nathan, “Sagedb: A learned database system,” in *CIDR*, 2019.

[32] B. Hilprecht, C. Binnig, and U. Röhm, “Towards learning a partitioning advisor with deep reinforcement learning,” in *aiDM@SIGMOD*, 2019, pp. 6:1–6:4.

[33] J. Ding, U. F. Minhas, B. Chandramouli, C. Wang, Y. Li, Y. Li, D. Kossmann, J. Gehrke, and T. Kraska, “Instance-optimized data layouts for cloud analytics workloads,” in *SIGMOD*. ACM, 2021, pp. 418–431.

[34] G. Moerkotte, “Small materialized aggregates: A light weight index structure for data warehousing,” in *VLDB*, 1998, pp. 476–487.

[35] Oracle, “Oracle documentation,” https://docs.oracle.com/en/.

[36] PostgreSQL, “Postgresql documentation,” https://www.postgresql.org/docs/.

[37] P. Larson, C. Clinciu, C. Fraser, E. N. Hanson, M. Mokhtar, M. Nowakiewicz, V. Papadimos, S. L. Price, S. Rangarajan, R. Rusanu, and M. Saubhasik, “Enhancements to SQL server column stores,” in *SIGMOD*, 2013, pp. 1159–1168.

[38] L. Sun, M. J. Franklin, J. Wang, and E. Wu, “Skipping-oriented partitioning for columnar layouts,” *PVLDB*, vol. 10, no. 4, pp. 421–432, 2016.

[39] F. C. Dictionary, “beam search http://foldoc.org/beam+search.”

[40] “OpenStreetMap dataset,” https://registry.opendata.aws/osm/.

[41] “Parquet Filter Pushdown,” https://drill.apache.org/docs/parquet-filter-pushdown/.